

UC Riverside

UC Riverside Previously Published Works

Title

Dispersion at the edges of near road noise barriers

Permalink

<https://escholarship.org/uc/item/04k4f82m>

Journal

Atmospheric Pollution Research, 12(2)

ISSN

1309-1042

Authors

Venkatram, Akula
Heist, David K
Perry, Steven G
[et al.](#)

Publication Date

2021-02-01

DOI

10.1016/j.apr.2020.11.017

Peer reviewed



EPA Public Access

Author manuscript

Atmos Pollut Res. Author manuscript; available in PMC 2022 February 05.

About author manuscripts

Submit a manuscript

Published in final edited form as:

Atmos Pollut Res. 2021 February 5; 12(2): 367–374. doi:10.1016/j.apr.2020.11.017.

Dispersion at the edges of near road noise barriers

Akula Venkatram^a, David K. Heist^{b,*}, Steven G. Perry^b, Lydia Brouwer^c

^aUniversity of California at Riverside, Riverside, CA, USA

^bUS Environmental Protection Agency, Research Triangle Park, NC, USA

^cJacobs Technology Inc., Research Triangle Park, NC, USA

Abstract

This paper presents an analysis of data from a wind tunnel study conducted to examine the dispersion of emissions at the edges of near-road noise barriers. The study is motivated by the concern that a barrier positioned downwind of a roadway may guide highly polluted plumes along the barrier leading to heightened concentrations as the plume spills around and downwind of the barrier end. The wind tunnel database consists of measurements of dispersion around a simulated roadway segment with various noise barrier configurations. Each roadway segment simulated in the wind tunnel had full-scale equivalent dimensions of 135 m long. Barrier segments, 135 m long with a height (H) of 6 m, were located on the downwind side of the source at a distance of 18 m from it (measured perpendicularly from the line source). Examination of the concentration patterns associated with the cases indicates that 1) vertical mixing induced by barriers persists at crosswind distances up to the edge (lateral end) of the barrier and downwind distances of $x/H = 10$, 2) concentration levels at all heights below $z/H = 1$ increase towards the edge of the barrier at downwind distances less than $x/H = 7$, and 3) concentration is well mixed in the vertical at the edge of the barrier, and the levels can be higher than in the middle of the barrier even when the source ends at the edge of the barrier. We have formulated a parameterization that captures the major features of these observations and can be incorporated in models such as RLINE.

Keywords

Near-road air quality; Dispersion modeling; Wind tunnel; Noise barriers; Edge effects

*Corresponding author. heist.david@epa.gov (D.K. Heist).

Credit author statement

Akula Venkatram, Conceptualization, Methodology, Software, Writing - original draft, Visualization. David K. Heist, Conceptualization, Methodology, Software, Investigation, Writing - review & editing, Visualization. Steve G. Perry, Conceptualization, Methodology, Investigation, Writing - review & editing, Visualization. Lydia Brouwer, Validation, Investigation, Resources, Data curation

Publisher's Disclaimer: Disclaimer

Publisher's Disclaimer: The U.S. Environmental Protection Agency through its Office of Research and Development funded and managed the research described here. The manuscript has been subjected to external peer review and has been cleared for publication. Although this work was reviewed by EPA and approved for publication, it may not necessarily reflect official agency policy. Mention of trade names or commercial products does not constitute endorsement or recommendation for use.

Declaration of competing interest

The authors declare that they have no known competing financial interests or personal relationships that could have appeared to influence the work reported in this paper.

1. Introduction

Epidemiological studies report associations between living within a few hundred meters of high-traffic roadways and adverse health effects such as asthma and other respiratory impacts, birth and developmental effects, premature mortality, cardiovascular effects, and cancer (Brauer et al., 2002; Finkelstein et al., 2004; Harrison et al., 1999; Hoek et al., 2002). This has motivated a number of studies on the impact of vehicular emissions on near-road air quality (e.g., Cohen et al., 2005; Hagler et al., 2009; Heist et al., 2009; Hitchins et al., 2000; Pirjola et al., 2006; Venkatram et al., 2007; Baldauf et al., 2013; Ranasinghe et al., 2019).

Field measurements (Baldauf et al., 2016; Finn et al., 2010), wind tunnel studies (Heist et al., 2009), and numerical simulations (Steffens et al., 2014; Gong and Wang, 2018) show that near-road barriers improve air quality downwind from roadways in most circumstances. Recent studies have explored the shape of the barrier (Wang and Wang, 2019), atmospheric stability (Reiminger et al. (2020)), and the effect of various combinations of barriers on either side of a roadway (Brechler and Fuka, 2014). Some of these results on the effects of barriers have been incorporated into conventional dispersion models (Ahangar et al., 2017; Schulte et al., 2014) used to examine the impact of highway emissions on near road air quality. However, these models do not address the behavior of highway emissions as they disperse around the barrier ends. Hagler et al. (2011) and Gong and Wang (2018) demonstrated through CFD modeling that a barrier positioned downwind of a roadway may guide highly polluted plumes along the barrier leading to heightened concentrations as the plume spills around and downwind of the barrier end.

To better understand these “edge effects”, the U. S. Environmental Protection Agency (U.S.EPA) performed a recent wind tunnel study to examine concentration patterns downwind of noise barriers of varying lengths and locations. This paper examines the data from the study to quantify these edge effects and suggests an algorithm to account for them that could be considered for inclusion within steady state dispersion models, such as RLINE (Snyder et al., 2013) or AERMOD (Cimorelli et al., 2005).

2. Wind tunnel study description

This database comprises wind tunnel measurements of tracer gas dispersion around a simulated roadway segment with various downwind noise barrier configurations. The study, conducted in the U.S. EPA’s open-circuit meteorological wind tunnel (Snyder, 1979), was designed to focus on the edge effects of noise barriers, i.e., the manner in which the pollutant emanating from the roadway source is dispersed over and around the end of the barrier.

2.1. Description of the model

At a model scale of 1:150, each roadway segment simulated in the wind tunnel had full-scale equivalent dimensions of 135 m long (see Fig. 1). The line source represents a single lane of traffic. Six-meter tall barrier segments (each 135 m long) were located on the downwind side of the source a distance of 18 m from it (measured perpendicularly from the source). The

barrier height, H , is the length scale used to normalize dimensions throughout the paper. The source segment and each barrier segment were therefore $22.5 H$ long.

The model roadway consisted of a single line source segment and noise barrier segments arranged in various configurations and at several angles to the wind direction. In all cases, the barrier was oriented parallel to the source line. The line source was constructed of a 90-cm length of 0.25-in. square thin-walled brass tubing. Holes, spaced one cm apart, were carefully drilled along the center of the downward face of the tubing providing a uniform release of tracer along the source tube. Five supply lines for the tracer gas were attached to the upwind face of the tubing and the ends of the tubing were plugged. The source gas was a mixture of pure ethane and air, with both gases provided to the system through mass flow controllers. The mass flow rate of ethane was set at 0.73 g/min and air was set at 2.4 g/min. Ethane, with a nearly equivalent molecular weight to that of air, mixed with air provided for a near-neutrally buoyant tracer. The barriers were constructed of thin, 0.1-cm, vertical steel plates.

2.2. Wind tunnel boundary layer

The boundary layer developed for this study was designed to simulate flow in a suburban area. A detailed description of the roughness configuration used to produce the boundary layer is found in Perry et al. (2016). The tunnel inlet air first encountered five Irwin spires (Irwin, 1981) positioned near the inlet of the test section. Immediately following the spires was an array of sharp-edged roughness tabs along the entire floor of the tunnel to condition and maintain the boundary layer throughout the test section. The tunnel ceiling was adjusted along the length of the test section to compensate for blockage effects due to the models and to allow a non-accelerating, free-stream flow. With a selected free-stream velocity of 4.7 m/s and the velocity profile from Perry et al. (2016), the full-scale surface roughness, z_0 , and friction velocity, u_* , were found to be 0.27 m and 0.25 m/s, respectively.

2.3. Wind tunnel measurement methods

Vertical, lateral, and longitudinal concentration profiles were measured by collecting tracer samples through the 0.24-cm outside-diameter brass tubes that were arranged in groups of six on vertical and horizontal sampling rakes mounted to the wind tunnel carriage. All samples were drawn through Beckman/Rosemount model 400 A hydrocarbon analyzers (flame ionization detectors) operating in the continuous sampling mode. Measured concentrations were normalized as $\chi = CU_o/(QL_xL_y)$, where C = measured concentration, U_o = reference wind speed (2.98 m/s) at the reference height, $z_{ref} = 20$ cm (30 m, full-scale), L_x is the along-wind dimension of the roadway segment (24 cm, 36 m full-scale), L_y is the cross-wind length of the roadway segment (90 cm, 135 m full scale) and Q = tracer mass emission rate (0.73 g/min). The tracer gas was high-purity ethane (C_2H_6) with a molecular weight of 30.07, only slightly heavier than air (29.97).

Calibrations were performed for the hydrocarbon analyzers everyday against a range of standardized gases. The samples were acquired at 20 Hz and averaged over 120 s. The concentration of the tracer gas was monitored over the measurement period and removed from the sample. This sampling protocol provide for reproducible mean concentrations with

an uncertainty of generally $\pm 5\%$, but as much as $\pm 10\%$ on the plume edges where variability is higher.

Laser Doppler velocimetry (LDV) was used to measure the velocity and turbulence profiles, to define the boundary layer characteristics. The LDV was a two-component, single-probe system that used the 488- and 514.5-nm lines from a Coherent Innova 70C argon-ion laser. The beam splitting, frequency shifting, and coupling of laser light to fiber-optic cables all were performed using a TSI Colorburst multicolor beam separator (model 9201, TSI Inc., St. Paul, MN, USA).

2.4. Cases considered

The cases considered here consist of tracer concentration measurements for a continuous release from a single line segment for winds perpendicular to the source and barrier. Dispersion patterns were characterized for flow with and without one or more noise barrier segments present. The first case (denoted “S1–B1”) is illustrated in Fig. 1 with the Source 1 running from $y/H = 0$ to 22.5 at $x/H = 0$ and Barrier 1 running from $y/H = 0$ to 22.5 at $x/H = 3$. Other cases discussed in this paper include “S1–B1,2” where an additional barrier is added which runs from $y/H = 22.5$ to 45 (see Fig. 3) and case “S2–B1” where a source runs from $y/H = -22.5$ to 0 (see Fig. 5) with Barrier 1. For each of the sources, we also consider cases without a barrier present. These are simply denoted “S1” and “S2” depending on the lateral location of the source. Measurements were performed at heights of $z/H = 0.25, 0.5, 1.0$ and 1.25 . Concentration profiles were measured at distances of $x/H = 2.5, 3.125, 3.5, 4, 5, 7, 10, 15,$ and 20 perpendicularly from the source. The measurements at $x/H = 2.5$ are between the source and the barrier; the associated concentrations are not discussed in this paper’s analysis of the impact of the barrier on dispersion.

3. Analysis of the data

3.1. Case S1–B1

We first consider the case of Source 1 with Barrier 1 (and the no barrier case S1) with the incident wind perpendicular to the source line. The associated concentration profiles comparing these two cases are shown in Fig. 2. Close to and just in the lee of the barrier at $x/H = 3.125$ and for $z/H < 0.5$, the concentrations near the middle of the barrier are lower than those in the absence of the barrier, as expected. The concentrations start increasing towards the edges at a distance of approximately $6.5H$ from the ends of the barriers. The concentration reaches a maximum at a lateral distance of about H beyond the edge of the barrier and then drops rapidly to zero. The concentration just downwind of the barrier ($x/H = 3.125$) is well mixed up to a height of $z/H = 1$ and then increases with height.

Fig. 2f, which shows the vertical concentration profiles at five locations along the barrier, indicate that the barrier mixes the concentrations in the vertical even near the edges of the barrier. The concentrations at these lateral locations in the presence of the barrier are above those in the absence of the barrier for all downwind distances. However, this result will be reexamined in comparison to the cases (see section 4.1) where the emissions from the line source were extended beyond the edge of the barrier (as in a more real-world simulation) so

that the concentrations in the absence of the barrier do not drop to zero. The important observation is that the near ground-level concentrations in the presence of the barrier begin to increase toward those in the absence of the barrier at about $6.5H$ from the edge. Furthermore, the vertical mixing by the barrier is effective almost to the edge of the barrier.

Concentration behavior at the edge of the barrier is important at both $z/H = 0.125$ and 0.5 because these heights bracket the breathing level. Fig. 2e shows that the barrier concentration at $z/H = 0.5$ approaches the no-barrier maximum concentration (at the edges of the barrier) more rapidly than it does at $z/H = 0.125$ at the edges of the barrier due in part to the increased vertical mixing by the barrier. Although somewhat difficult to estimate, the lateral location at which the concentration begins to increase towards the no-barrier maximum also occurs at approximately $6.5H$ from the barrier edge. The S1–B1,2 case (with source 1 and barriers 1 and 2), considered in section 3.2, provides more information on this transition.

Fig. 2h shows that at $x/H = 10$, the edge effect is not apparent, while Fig. 2g indicates that there is diminishing difference between the barrier and no-barrier cases beyond $x/H = 10$. Note that vertical mixing induced by the barrier is evident even at this distance (Fig. 2i). Fig. 2f shows the impact of the barrier on the vertical profiles of concentrations at various crosswind distances from the center of the source at $x/H = 3.125$. In Fig. 2c, we see that in the absence of the barrier, the concentration decreases with height as expected, and the levels are lower at the edges of the source ($y/H = 0.25$ and 22.25) than in the middle ($y/H = 11.25$). In the presence of the barrier, the concentration is well mixed in the vertical across most of the plume. However, the concentrations at all levels up to the height of the barrier are higher at the edges of the plume at $y/H = 0.25$ and 22.25 than those at the middle of the plume at $y/H = 6.25$ and 16.25 . This increase in concentrations towards the edges of the barrier is clearly related to flow around the edges of the barrier.

We next examine S1–B1,2 case in which the edge effects are important at only one end of the barrier.

3.2. Source 1 with barriers 1 & 2

In the S1–B1,2 case, consisting of source 1 along with the two sections of barrier depicted in Fig. 3, we expect to see edge effects only at the $y/H = 0$ end of Barrier 1.

We notice that, as in S1–B1 case, the barrier concentration approaches the maximum no-barrier concentration very close to the edge of the barrier (See Fig. 4b). This suggests that for $z/H = 0.5$, concentration in the presence of the barrier starts increasing around $6.5H$ from the edge of the barrier, and transitions to a level that is close to the no-barrier maximum close to end of the barrier. It should also be noted that the vertical mixing induced by the barrier is still apparent at the edge.

In Fig. 4d through 4f we contrast the concentrations for cases S1–B1 and S1–B1,2. Near the center of Barrier 1, the concentrations are very similar for both cases for all downwind distances (Fig. 4d). In fact, for a large part of Barrier 1 ($0 < y < 15H$), the concentrations are similar for both cases (Fig. 4e). However, as transition from Barrier 1 to Barrier 2 is

approached at $y/H = 22.5$, the edge effect (increase in concentration followed by a sharp decrease) seen in S1–B1 disappears and the concentration just downwind of the barriers slowly drops off to zero as Barrier 2 directs some of the flow along the barrier.

Fig. 4c, f and h, which shows the vertical concentration profiles at $x/H = 3.125$ and $x/H = 10$, indicates that the barrier is effective in mixing the plume in the vertical. It is significant that at $x/H = 3.125$, the concentrations at the edge of the barrier at $y/H = 0$ are higher than those close to the middle of the barrier up to a height of $z/H = 1$. This behavior is related to the flow around the edge of Barrier 1. At $x/H = 10$, the concentrations at the edges of the plume are smaller than those in the middle of the plume.

3.3. Source 2 with barrier 1

Case S2–B1 examines the effect of the flow induced by Barrier 1 on the concentration pattern associated with emissions from the source segment with a barrier offset laterally (Fig. 5).

We see from Fig. 6c that the presence of Barrier 1 with Source 2 alters the vertical concentration profile at $y/H = -0.25$ corresponding to the edge of the barrier: the plume is well mixed in the vertical. Furthermore, the concentrations do not decrease monotonically with downwind distance as in the no barrier case, S2 (see Fig. 6d). It is clear that the flow induced by barrier edges has a significant effect on concentrations downwind of the barrier. Additionally, in Fig. 6b for the side of the plume closer to the barrier (near $y/H = 0$), the flow around the barrier end pushes the vertically well-mixed plume slightly in the negative- y direction as can be seen in the faster drop off in concentration for the S2–B1 case than for the no barrier case.

3.4. Lessons from the analysis of wind tunnel data

Examination of the concentration patterns associated with the cases described in the preceding sections leads to the following conclusions on dispersion of line source emissions at the ends of near road barriers:

1. The vertical mixing induced by barriers persists at crosswind distances up to the edge of the barrier and downwind distances up to $x/H = 10$ and possibly beyond.
2. The concentration levels at all heights below $z/H = 1$ increase towards the edge of the barrier for downwind distances close to the barrier (see for example, Fig. 2f). This is related to the flow around the ends of the barrier.
3. The concentration is well mixed in the vertical at the edge of the barrier, and the levels can be higher than in the middle of the barrier even though the source ends at the edge of the barrier. This suggests that a portion of the vertically mixed plume material travels laterally along the upwind side of the barrier before moving downwind at the edge.
4. The plume emanating from a segment of roadway laterally offset from a barrier (e.g., case S2–B1) is deflected laterally away from the end of barrier by the winds moving around the end (see Fig. 6b near $y/H = 0$).

In light of the findings from the wind tunnel study, it is useful to formulate a model that incorporates the effects on a line source of the barrier edge into a dispersion model, such as RLINE. The model has the potential to serve as a computational tool for regulatory applications and for designing mitigation strategies based on noise barriers.

4. Dispersion model with edge effects for perpendicular wind

We first describe a dispersion model that accounts for barrier effects but does not account for edge effects.

As shown in Fig. 7, the barrier mixes the plume below the barrier height. Above the barrier, the concentration distribution is taken to be that in the absence of the barrier scaled by a factor, f_q . Then, the concentration below the barrier is the value of this scaled concentration distribution at $z = 0$, where the $z = 0$ plane is taken to be the top of the barrier. Then, the scaling factor, f_q , can be derived from a simple mass balance,

$$f_q = \frac{1}{U_b H C_q(x, 0) + 1} \quad (1)$$

where U_b the wind speed used to advect the plume material below H and is taken to be half the velocity at the top of the barrier. $C_q(x, 0)$ is the crosswind integrated concentration per unit emission rate in the absence of the barrier,

$$C_q(x, z) = \frac{1}{\sqrt{2\pi}\sigma_z U_{eff}} \left(\exp\left(-\frac{1}{2}\left(\frac{z - z_s}{\sigma_z}\right)^2\right) + \exp\left(-\frac{1}{2}\left(\frac{z + z_s}{\sigma_z}\right)^2\right) \right) \quad (2)$$

where σ_z is the vertical plume spread, z is the receptor height relative to the barrier height, and z_s is the source height. The vertical plume spread, σ_z , and the effective velocity, U_{eff} , are computed using the formulations in RLINE (Snyder et al., 2013; Venkatram et al., 2013) and the meteorological variables above the barrier.

The concentration below $z = H$ is simply $f_q q C_q(x, 0)$, and above the barrier it is $f_q q C_q(x, z)$, where q is the emission per unit length of the source. Notice that when $H = 0$ in the absence of the barrier, we recover the correct concentration profile because $f_q = 1$. We account for the finite length of the source by multiplying the concentration distribution by the factor (Venkatram and Horst, 2006):

$$F_h = \frac{\text{erf}(t_1) - \text{erf}(t_2)}{2} \quad (3)$$

$$t_i = \frac{Y_i - Y_r}{\sqrt{2}\sigma_y(X_r)}$$

where erf is the error function, X_r and Y_r are the receptor co-ordinates in a co-ordinate system in which the Y -axis lies along the source, and Y_1 and Y_2 are the co-ordinates of the ends of the line source. We account for edge effects by allowing the concentration to increase towards the edge as shown in Fig. 8.

Based on the observations made in the wind tunnel, we assume that the concentrations below the barrier height increase linearly as a function of crosswind spread as shown in Fig. 8 and remains constant with height. We obtain adequate fits to the measured concentrations if we take $Y_L = 2.5H$, $Y_U = 6.5H$ and $C_{max} = 0.9C_{nb}$.

In addition, for a road segment adjacent to but not directly upwind of a barrier (e.g., case S2–B1), the length of the source is shortened by a length equal to one barrier height (i.e., H) on the end of the source closer to the end of the barrier. This accounts for the lateral deflection of the plume as the wind moves around the edge of the barrier. The emissions from this segment of roadway are added to the remainder of the road segment to preserve the total emissions.

4.1. Comparison with wind tunnel for 90°

Fig. 9 shows the performance of these parameterizations in describing the concentrations affected by the barrier edge for cases S2–B1 and S1–B1,2 (see Figs. 3 and 5 for configuration schematics). We see that the model provides an adequate description of the lateral distributions at $x/H = 3.125, 5, \text{ and } 10$.

For the S2–B1 case (Fig. 9 a, d and g), the model and the observations both show an earlier drop off in concentration near $y/H = 0$ compared to the drop off near $y/H = -22.5$.

The lateral profiles for the S1–B1,2 case (Fig. 9 b and e) display the main effect of the end of the barrier, namely the rise in concentration as the end of the barrier is approached (near $y/H = 0$). Furthermore, the model correctly predicts that at the edge $y/H = 0$, the concentration in the presence of the barrier is larger than that in the absence of barrier. These figures indicate that the observations at $y/H = 11.25$ are not affected by the edge. The model performs well in describing the downwind variation of the concentration along the center of the sources.

Fig. 9h shows that the edge effect is not apparent in the observations at $x/H = 10$. From an examination of all the data for these cases, the edge effects appear to drop off after $x/H = 7$. Therefore, to account for the lack of observed edge effects at relatively large distances from the source, the edge correction is applied only for distances $x/H < 7$. This limit is reflected in the model predictions at $x/H = 10$ (Fig. 9h). Fig. 9c and f indicate that the modeled concentration is not mixed in the vertical at the edge of the barrier at $y/H = 1.25$, although the levels near the surface are close to the observations, and the model correctly predicts that the concentrations at the edge of the barrier are higher in the presence of the barrier than those in the absence of the barrier (e.g., compare Figs. 9b to 7b). The lack of vertical well-mixedness in the model is due to the blending of the barrier/no-barrier cases.

To examine the interaction of these algorithm elements when a continuous stretch of highway is modeled that includes a barrier end, we combine the two cases shown in Fig. 9. Each result from Fig. 9 is reproduced in Fig. 10 (the red and blue lines), with the results of the elements now superposed to create the effect of the continuous length of roadway (the black line). The lateral profile of the observations was also created from the individual cases.

The modeled concentration for the combined roadway segments reproduces well the observed concentrations near the surface ($z/H = 0.125$). At greater heights, a more refined treatment of the effect of the barrier will be required to capture the observed well-mixed nature that extends even near the end of barrier.

4.2. Observations on modeling approach

The parameterization presented in the previous section provides an adequate description of the main features of the edge effects observed in the wind tunnel. It describes:

1. The increase in the near surface downwind concentration towards the barrier edge. The maximum concentration at the edge of the barrier is approximately $C_{nb} - 0.3(C_{nb} - C_b)$, where C_{nb} is the centerline concentration in the absence of the barrier, and C_b is the centerline concentration in the presence of the barrier. The concentration starts increasing at about $6.5H$ from the edge of the barrier, where H is the height of the barrier.
2. The deflection of a plume emanating from a segment of roadway adjacent to the end of a barrier.
3. The absence of noticeable edge effects beyond a downwind distance of seven times the barrier height.

5. Summary and conclusions

We present an analysis of data from a wind tunnel study conducted to examine the dispersion of emissions at the edges of near-road noise barriers motivated by concern that heightened downwind concentrations may occur as the plume spills around the end of the barrier. The analysis is limited to the case where winds are perpendicular to the roadway, though further exploration of oblique winds is necessary before drawing conclusions about wind direction. We observed that vertical mixing downwind of the barrier persists at crosswind distances up to the edge of the barrier for downwind distances less than $10H$. Surface levels of concentration downwind of the barrier are generally lower than those without a barrier though they do increase as the end of the barrier is approached. The flow around the end of the barrier tends to modestly deflect the emissions from segments of roadway extending beyond the barrier in the direction away from the barrier.

A model is proposed to account for these effects and is shown to perform reasonably well against near surface concentrations from the wind tunnel measurements. This model accounts for the increase in concentration as the end of the barrier is approached and the deflection of emissions from the segment of roadway adjacent to but beyond the barrier end. More refinement in the algorithm is needed to capture the observed vertically well-mixed region that extends to near the end of barrier.

References

- Ahangar FE, Heist DK, Perry S, Venkatram A, 2017. Reduction of air pollution levels downwind of a road with an upwind noise barrier. *Atmos. Environ* 155, 1–10. 10.1016/j.atmosenv.2017.02.001.

- Baldauf RW, Heist DK, Isakov V, Perry SG, Hagler GW, Kimbrough S, Shores R, Black K, Brixey L, 2013. Air quality variability near a highway in a complex urban environment. *Atmos. Environ* 64, 169–178. 10.1016/j.atmosenv.2012.09.054.
- Baldauf R, Iskov V, Deshmarkh P, Venkatram A, Yang B, Zhang KM, 2016. Influence of solid noise barriers on near-road and on-road air quality. *Atmos. Environ* 129, 265–276.
- Brauer M, Hoek G, Van Vliet P, Meliefste K, Fischer PH, Wijga A, Koopman LP, Neijens HJ, Gerritsen J, Kerkhof M, Heinrich J, Bellander T, Brunekreef B, 2002. Air pollution from traffic and the development of respiratory infections and asthmatic and allergic symptoms in children. *Am. J. Respir. Crit. Care Med* 166, 1092–1098. 10.1164/rccm.200108-007OC. [PubMed: 12379553]
- Brechler J, Fuka V, 2014. Impact of noise barriers on air-pollution dispersion. *Nat. Sci* 6, 337–386.
- Cimorelli AJ, Perry SG, Venkatram A, Weil JC, Paine RJ, Wilson RB, Lee RF, Peters WD, Brode RW, 2005. AERMOD: a dispersion model for industrial source applications. Part I: general model formulation and boundary layer characterization. *J. Appl. Meteorol* 44, 682–693. 10.1175/JAM2227.1.
- Cohen J, Cook R, Bailey CR, Carr E, 2005. Relationship between motor vehicle emissions of hazardous pollutants, roadway proximity, and ambient concentrations in Portland, Oregon. *Environ. Model. Software* 20, 7–12. 10.1016/j.envsoft.2004.04.002.
- Finkelstein MM, Jerrett M, Sears MR, 2004. Traffic air pollution and mortality rate advancement periods. *Am. J. Epidemiol* 160, 173–177. 10.1093/aje/kwh181. [PubMed: 15234939]
- Finn D, Clawson KL, Carter RG, Rich JD, Eckman RM, Perry SG, Isakov V, Heist DK, 2010. Tracer studies to characterize the effects of roadside noise barriers on near-road pollutant dispersion under varying atmospheric stability conditions. *Atmos. Environ* 44, 204–214. 10.1016/j.atmosenv.2009.10.012.
- Gong L, Wang X, 2018. Numerical study of noise barriers' side edge effects on pollutant dispersion near roadside under various thermal stability conditions. *Fluid* 3, 105. 10.3390/fluids3040105.
- Hagler GSW, Tang W, Freeman MJ, Heist DK, Perry SG, Vette AF, 2011. Model evaluation of roadside barrier impact on near-road pollution. *Atmos. Environ* 45, 2522–2530.
- Hagler GSW, Baldauf RW, Thoma ED, Long TR, Snow RF, Kinsey JS, Oudejans L, Gullett BK, 2009. Ultrafine particles near a major roadway in Raleigh, North Carolina: downwind attenuation and correlation with traffic-related pollutants. *Atmos. Environ* 43, 1229–1234. 10.1016/j.atmosenv.2008.11.024.
- Harrison RM, Leung PL, Somerville L, Smith R, Gilman E, 1999. Analysis of incidence of childhood cancer in the West Midlands of the United Kingdom in relation to proximity to main roads and petrol stations. *Occup. Environ. Med* 56, 774–780. 10.1136/oem.56.11.774. [PubMed: 10658564]
- Heist DK, Perry SG, Brixey L.a., 2009. A wind tunnel study of the effect of roadway configurations on the dispersion of traffic-related pollution. *Atmos. Environ* 43, 5101–5111. 10.1016/j.atmosenv.2009.06.034.
- Hitchins J, Morawska L, Wolff R, Gilbert D, 2000. Concentrations of submicrometre particles from vehicle emissions near a major road. *Atmos. Environ* 34, 51–59. 10.1016/S1352-2310(99)00304-0.
- Hoek G, Brunekreef B, Goldbohm S, Fischer P, van den Brandt PA, 2002. Association between mortality and indicators of traffic-related air pollution in The Netherlands: a cohort study. *Lancet* 360, 1203–1209. 10.1016/S0140-6736(02)11280-3. [PubMed: 12401246]
- Irwin HPAH, 1981. The design of spires for wind simulation. *J. Wind Eng. Ind. Aerod* 7, 361–366. 10.1016/0167-6105(81)90058-1.
- Perry SG, Heist DK, Brouwer LH, Monbureau EM, Brixey LA, 2016. Characterization of pollutant dispersion near elongated buildings based on wind tunnel simulations. *Atmos. Environ* 142, 286–295.
- Pirjola L, Paasonen P, Pfeiffer D, Hussein T, Hämeri K, Koskentalo T, Virtanen A, Rönkkö T, Keskinen J, Pakkanen TA, Hillamo RE, 2006. Dispersion of particles and trace gases nearby a city highway: mobile laboratory measurements in Finland. *Atmos. Environ* 40, 867–879. 10.1016/j.atmosenv.2005.10.018.
- Ranasinghe D, Lee ES, Zhu Y, Frausto-Vicencio I, Choi W, Sun W, Mara S, Seibt U, Paulson SE, 2019. Effectiveness of vegetation and sound wall-vegetation combination barriers on pollution

- dispersion from freeways under early morning conditions. *Sci. Total Environ* 658, 1549–1558. [PubMed: 30678013]
- Reiminger N, Jurado X, Vazquez J, Wemmert C, Blond N, Dufresne M, Wertel J, 2020. Effects of wind speed and atmospheric stability on the air pollution reduction rate induced by noise barriers. *J. Wind Eng. Ind. Aerod* 200, 104160. 10.1016/j.jweia.2020.104160.
- Schulte N, Snyder M, Isakov V, Heist D, Venkatram A, 2014. Effects of solid barriers on dispersion of roadway emissions. *Atmos. Environ* 97, 286–295. 10.1016/j.atmosenv.2014.08.026.
- Snyder MG, Venkatram A, Heist DK, Perry SG, Petersen WB, Isakov V, 2013. RLINE: a line source dispersion model for near-surface releases. *Atmos. Environ* 77, 748–756. 10.1016/j.atmosenv.2013.05.074.
- Snyder WH, 1979. The EPA Meteorological Wind Tunnel: its Design, Construction, and Operating Characteristics. U.S. Environmental Protection Agency, Research Triangle Park, NC Report No. EPA-600/4-79-051.
- Steffens JT, Heist DK, Perry SG, Isakov V, Baldauf RW, Zhang KM, 2014. Effects of roadway configurations on near-road air quality and the implications on roadway designs. *Atmos. Environ* 94, 74–85. 10.1016/j.atmosenv.2014.05.015.
- Venkatram A, Horst TW, 2006. Approximating dispersion from a finite line source. *Atmos. Environ* 40, 2401–2408. 10.1016/j.atmosenv.2005.12.014.
- Venkatram A, Isakov V, Thoma E, Baldauf R, 2007. Analysis of air quality data near roadways using a dispersion model. *Atmos. Environ* 41, 9481–9497. 10.1016/j.atmosenv.2007.08.045.
- Venkatram A, Snyder MG, Heist DK, Perry SG, Petersen WB, Isakov V, 2013. Re-formulation of plume spread for near-surface dispersion. *Atmos. Environ* 77, 846–855. 10.1016/j.atmosenv.2013.05.073.
- Wang S, Wang X, 2019. Modeling and analysis of the effects of noise barrier shape and inflow conditions on highway automobiles emission dispersion. *Fluid* 4, 151. 10.3390/fluids4030151.

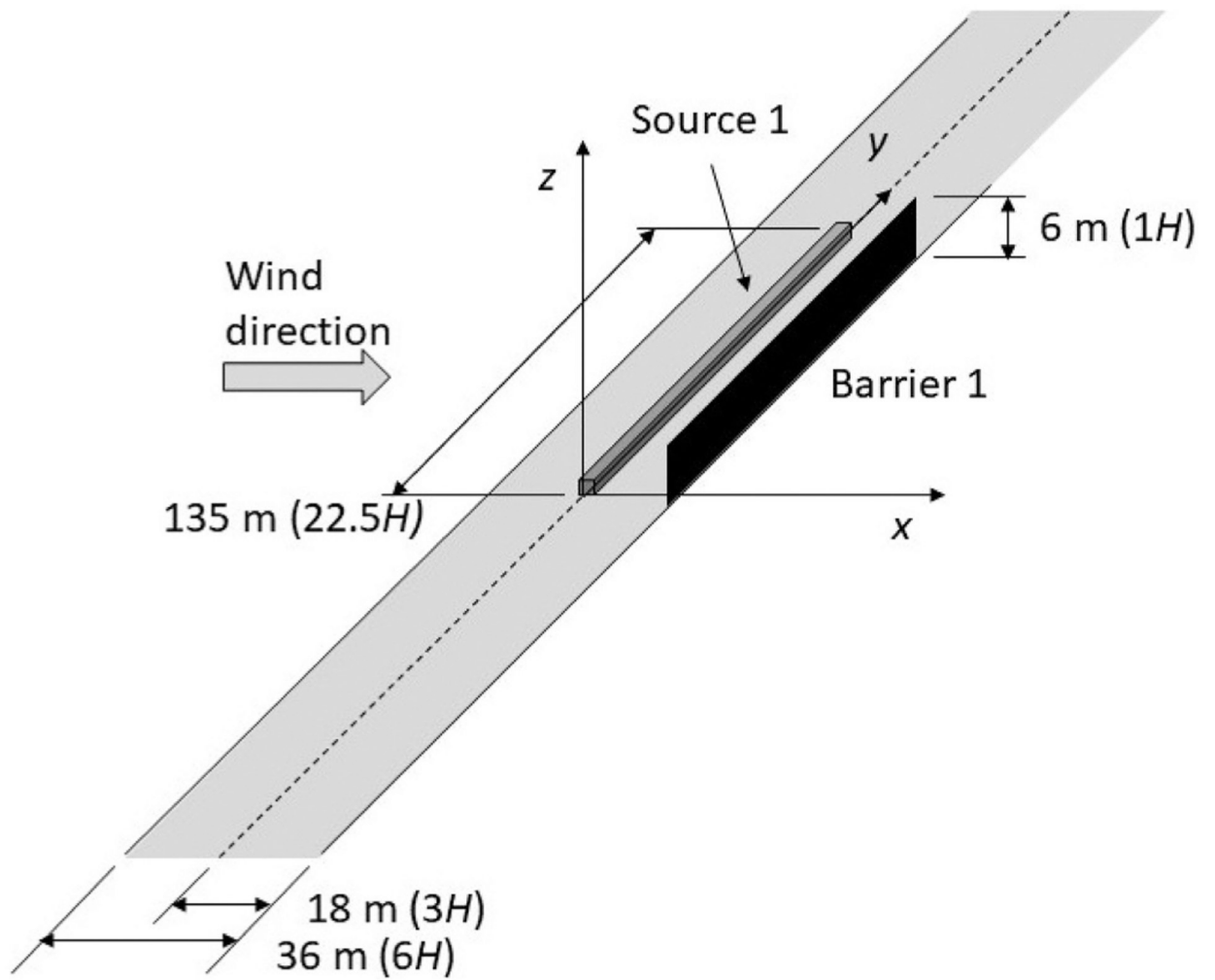


Fig. 1. Source-barrier configuration for case S1-B1. The source and barrier run from $y/H = 0$ to 22.5 . The source is located at $x/H = 0$, while the barrier is at $x/H = 3$. The barrier height ($1H$) is 6 m at full-scale.

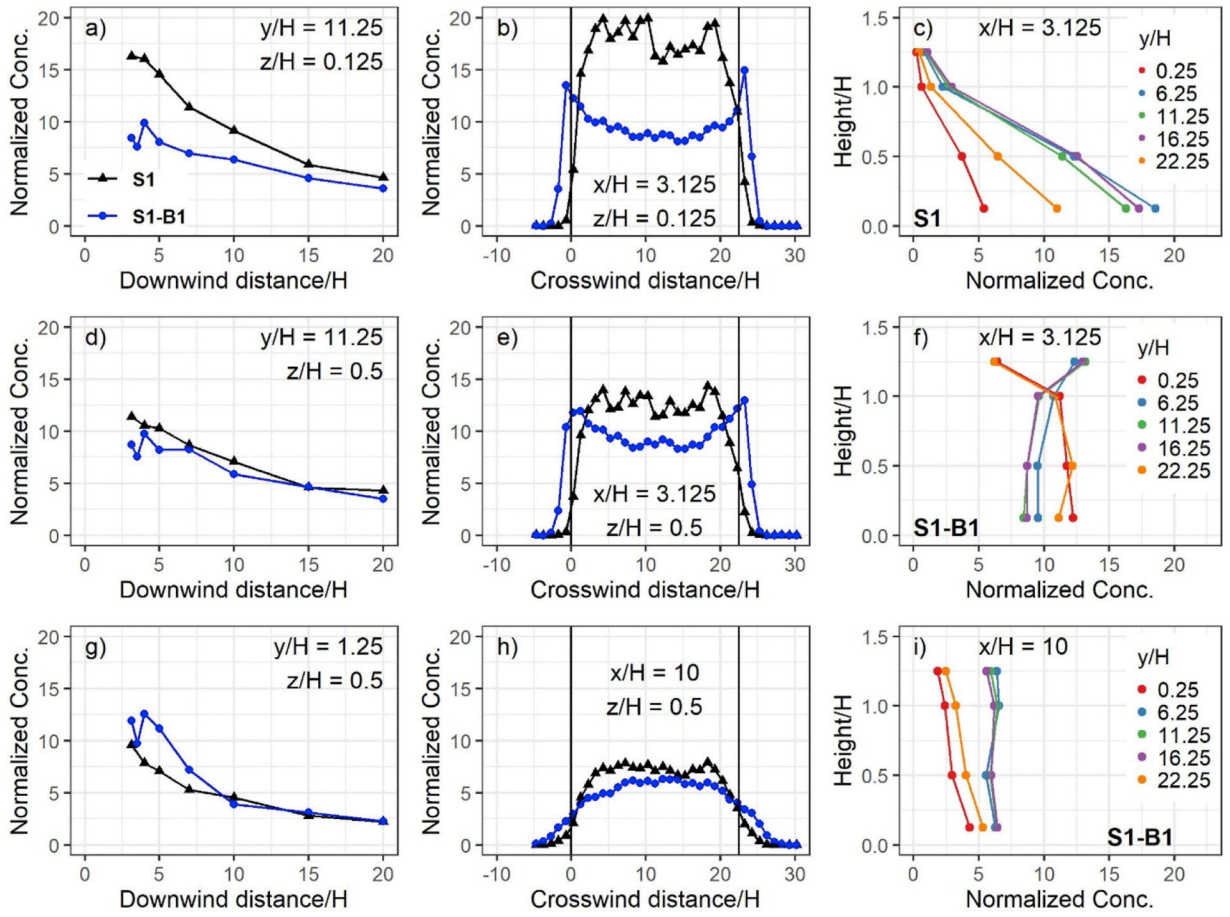


Fig. 2.
 Comparison of Source 1 no barrier (S1) and barrier 1 (S1-B1) cases. The vertical lines in Figures b, e, and h indicate the beginning and end of the barrier at $y/H = 0$ and 22.5 .

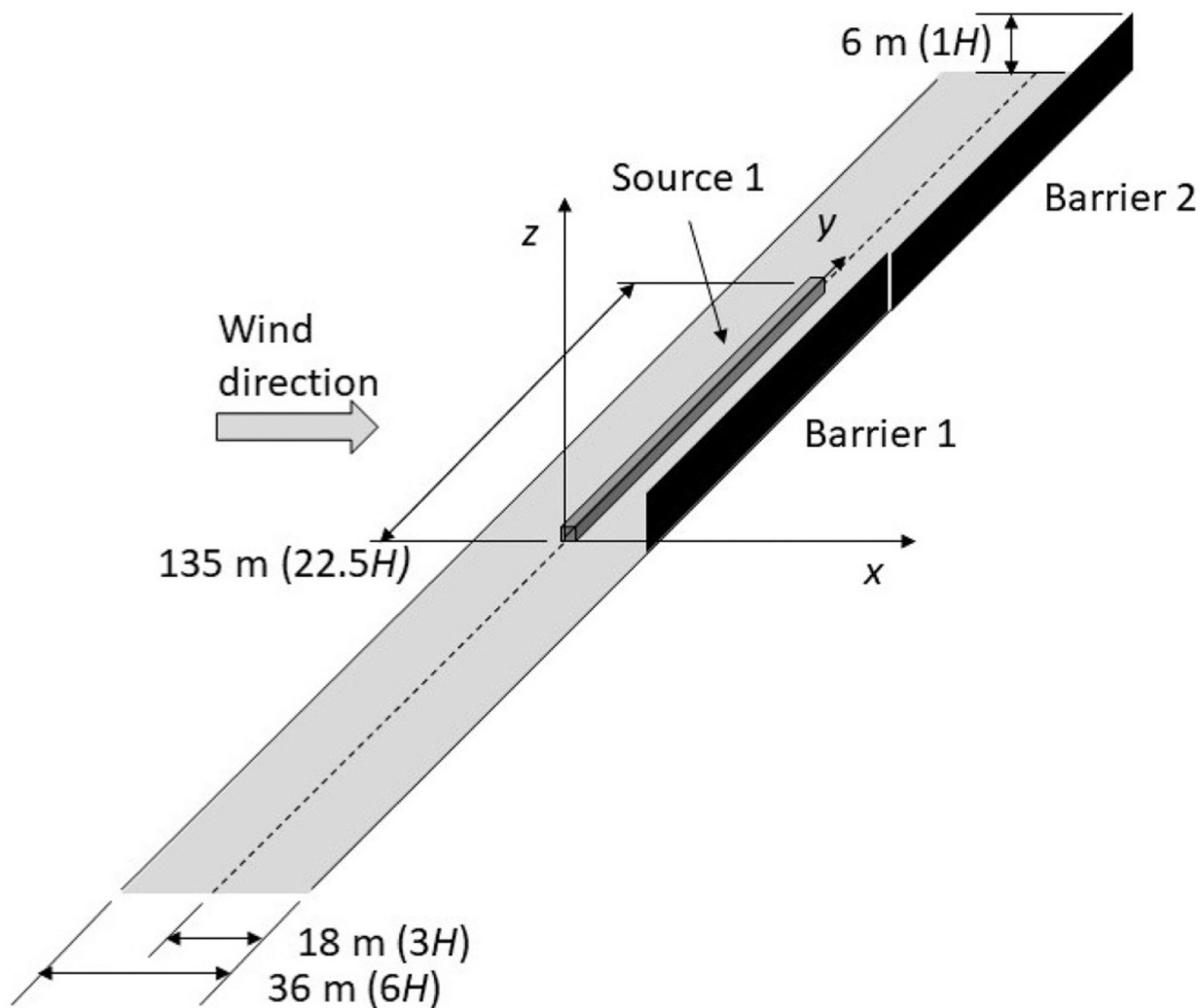


Fig. 3.
Source-barrier configuration for case S1-B1,2.

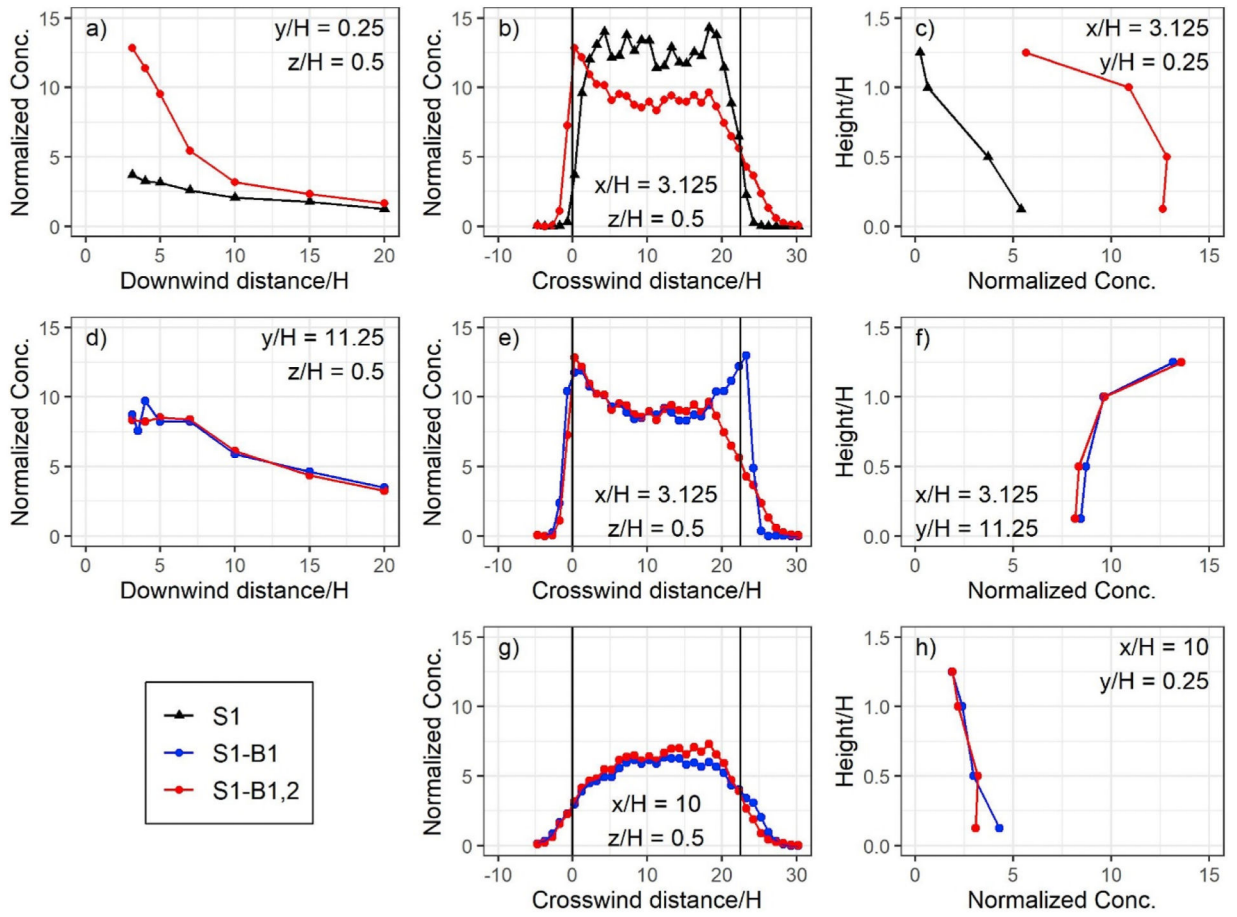


Fig. 4. Comparison of Source 1 no barrier (S1 NB) and the Source 1 with barriers 0 & 1 (S1 B01) cases (a through c). Comparison of S1 B1 case with the S1 B01 case (d through h).

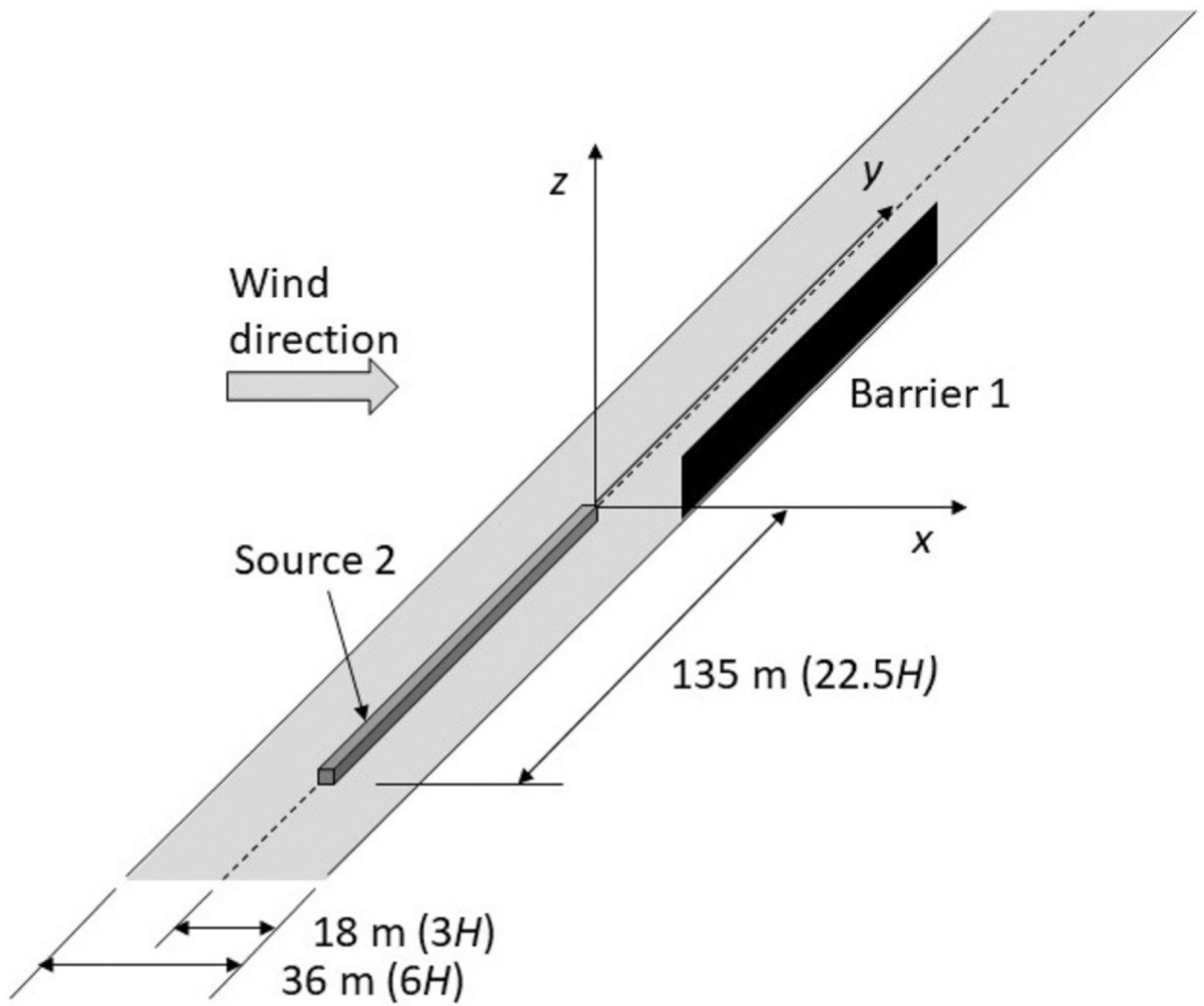


Fig. 5. Source-barrier configuration for case S2-B1.

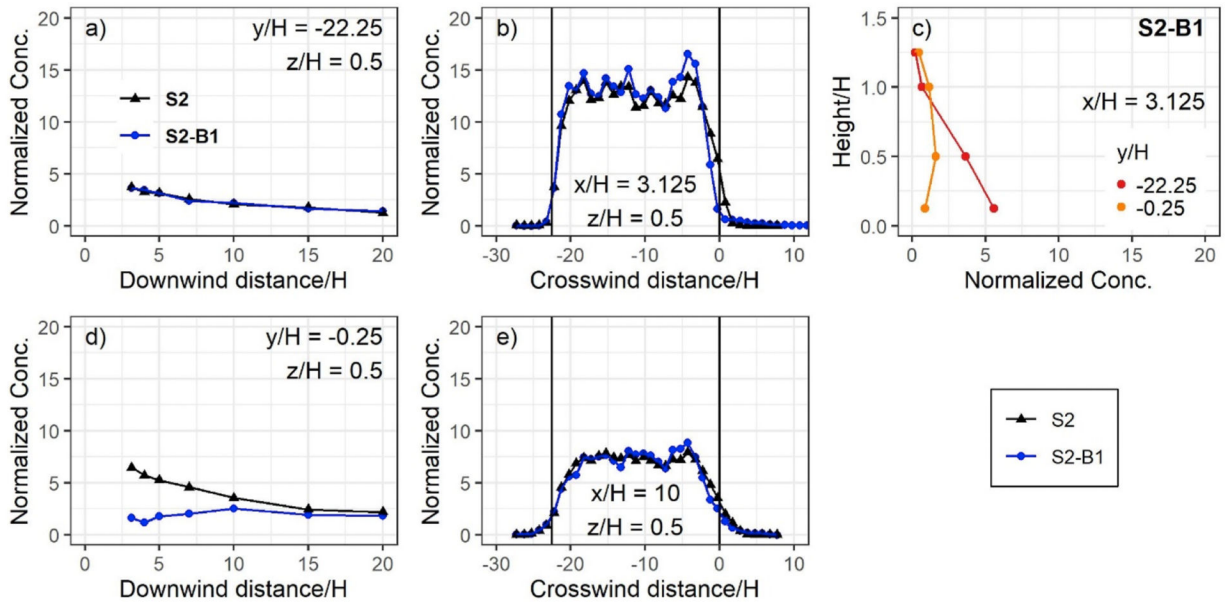


Fig. 6.
Comparison of Source 2 no barrier (S2) and the Source 2 with Barrier 1 (S2-B1).

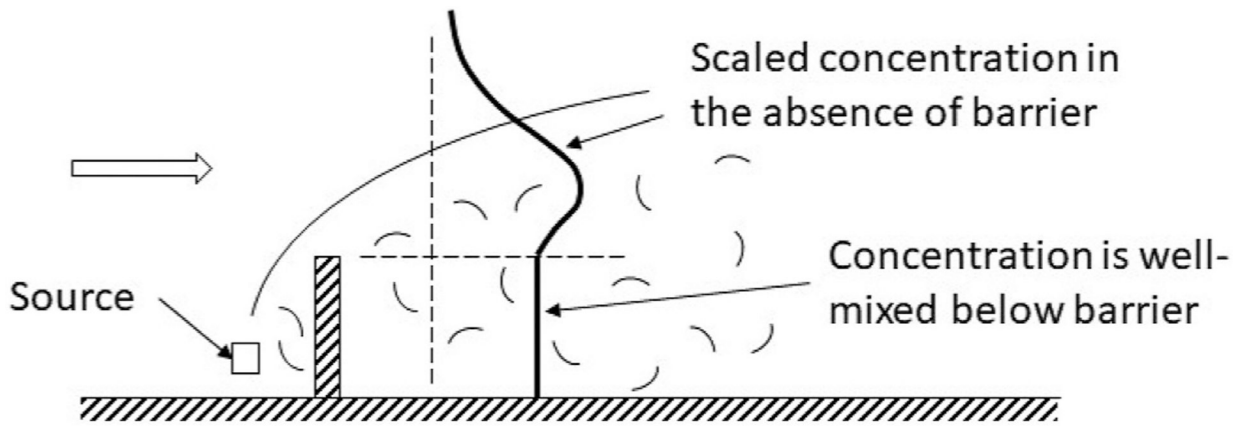


Fig. 7. Schematic used to derive dispersion model that accounts for barrier effect.

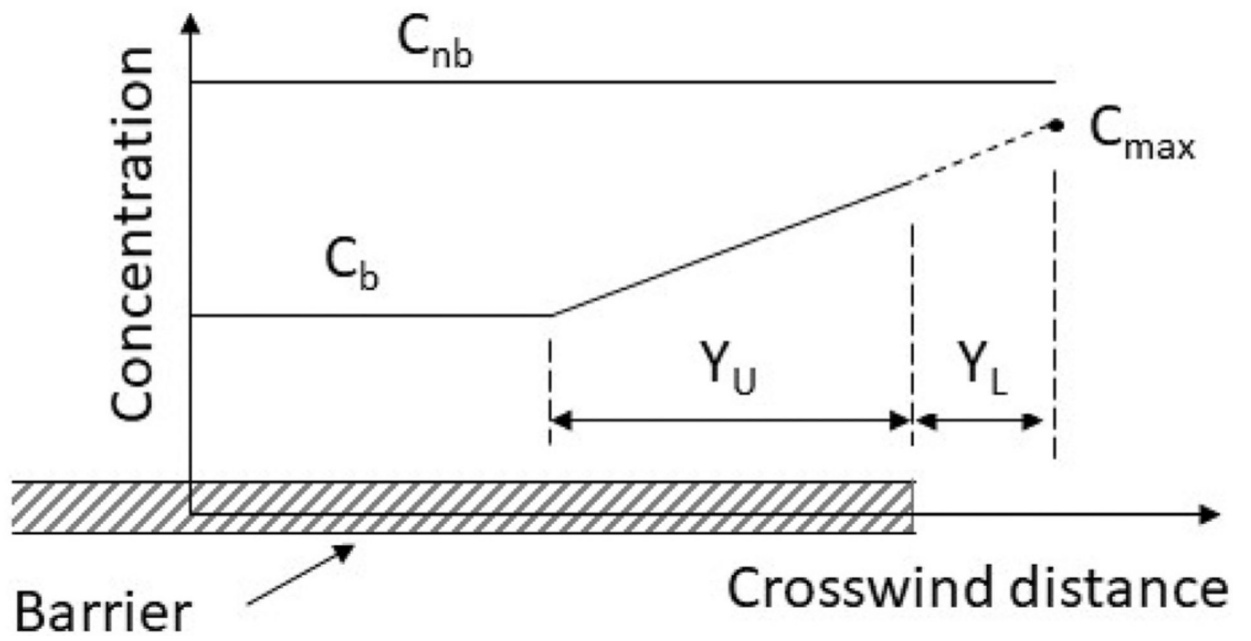


Fig. 8.
Schematic used to derive dispersion model that accounts for barrier effects.

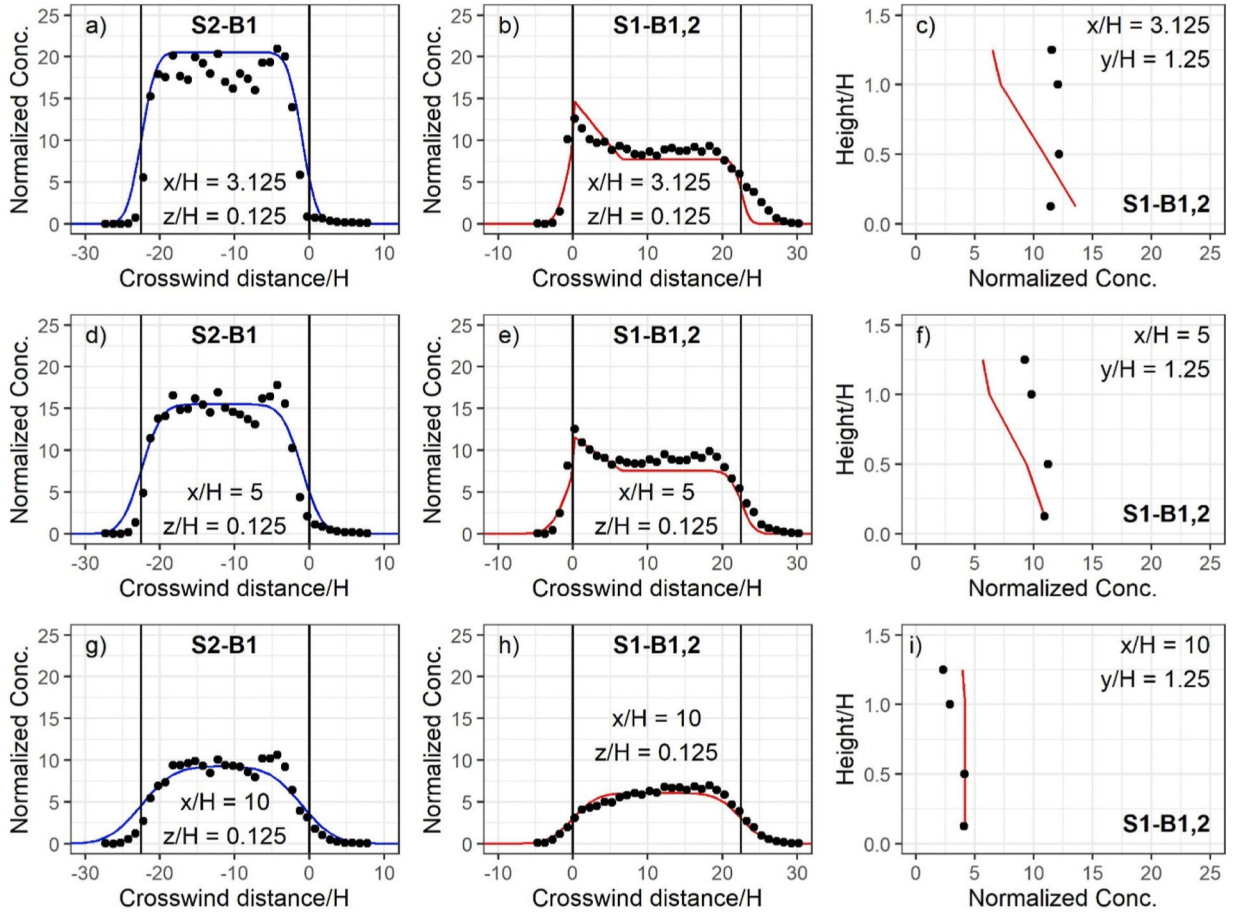


Fig. 9. Performance of parameterization for the Barrier P and Barrier 0 P cases at downwind distances of $x/H = 3.125, 5$ and 10 . Lines indicate model results parameterized for barrier effects; black circles are wind tunnel results.

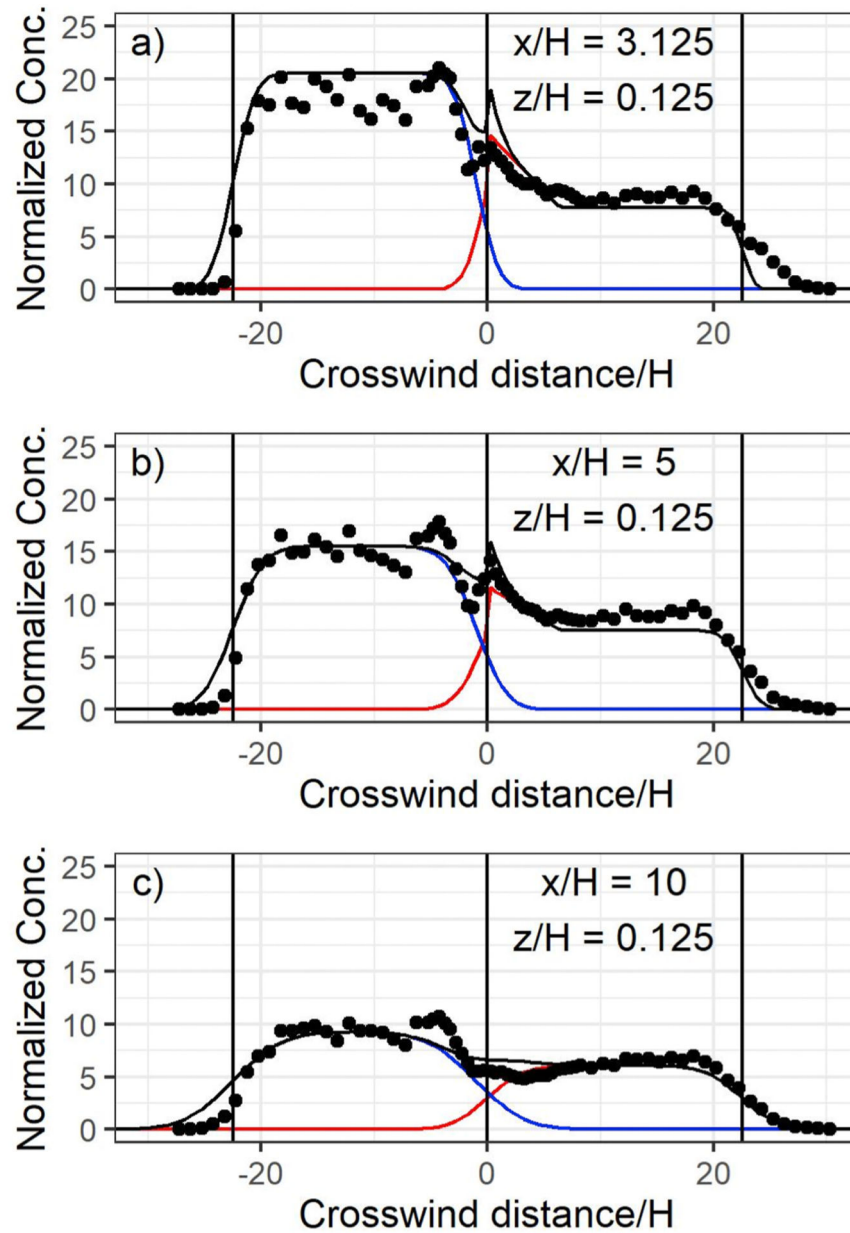


Fig. 10. Performance of parameterization for the combined S1–B1,2 and S2–B1 cases at downwind distances of $x/H = 3.125, 5$ and 10 . Red and blue lines indicate model results for S1–B1,2 and S2–B1, respectively; black lines indicate superposition of individual cases; black circles are wind tunnel results for superposed cases.